Synthesis of quadrangular bismuth oxychloride NFs for the reduction of 4-NP and the degradation of rhodamine B

Ya Liu ✉, *Yuqing Miao*

Institute of Bismuth Science, University of Shanghai for Science and Technology, Shanghai 200093, People's Republic of China
✉ *E-mail: 834077335@qq.com*

Published in Micro & Nano Letters; Received on 23rd October 2018; Revised on 22nd December 2018; Accepted on 15th January 2019

The quadrangular (QA) bismuth oxychloride nanoflakes (NFs) were synthesised by a simple solvothermal reaction. They were characterised by scanning electron microscope, transmission electron microscope and X-ray diffractometer. As catalysts, the square NFs exhibited excellent catalytic performance in the reduction of 4-nitrophenol (4-NP) and the degradation of rhodamine B (RhB). The complete reduction of 4-NP to 4-aminophenol was obtained in 30 s and the nearly complete degradation of RhB in 20 min.

1. Introduction: Bismuth oxychloride (BiOCl) is a highly anisotropic layered structure with excellent physical and chemical properties [1–5]. It is also the first synthetic non-toxic pearlescent pigment. BiOCl is widely used in photocatalysts [1, 6–10], gas sensitive materials and pearlescent pigments [11]. Moreover, the specific structure, morphology and composition of BiOCl have different optical, electrical and catalytic properties [12, 13].

It is well known that 4-nitrophenol (4-NP) is a toxic organic compound. It is also an intermediate for fine chemicals such as dyes and pharmaceuticals [14]. Therefore, 4-NP is one of many pollutants in wastewater. It is very difficult to degrade 4-NP under natural conditions [15, 16]. The product obtained after the reduction of 4-NP is p-aminophenol (4-AP), and the resulting 4-AP not only has a much reduced toxicity, but also occupies an important position in the chemical industry [17–19]. The main methods to remove 4-NP are physical methods such as adsorption and chemical methods such as microwave-assisted catalytic oxidation, photocatalytic degradation and electrochemistry. However, these methods consume a lot of energy, and some of them need to be carried out in organic solvents. Therefore, it is necessary to study the degradation of 4-NP in water. However, the reduction of 4-NP by sodium borohydride ($NaBH_4$) catalysed by BiOCl has not been reported.

Photocatalytic technology is considered to be a highly environmentally friendly and economical way to treat pollutants [7, 20, 21]. At present, the study of BiOCl is mainly focused on photocatalysis due to its excellent photocatalytic performance under ultraviolet (UV) light and visible light conditions [22–24]. It is reported that controlling the composition and structure of crystal can improve the photocatalytic performance [8].

In this work, QA-BiOCl-nanoflakes (NFs) were synthesised by simple solvothermal method without surfactant. QA-BiOCl-NFs showed double catalytic function here. It can reduce 4-NP and degrade rhodamine B (RhB). QA-BiOCl-NF has the advantages of low cost, high catalytic activity and environmental protection.

2. Experimental section

2.1. Reagents: Bismuth nitrate pentahydrate ($Bi(NO_3)_3{\cdot}5H_2O$), HCl, $NaBH_4$, RhB, 4-NP, ethylene glycol and hydrogen peroxide (H_2O_2) solution (purity≃30%) were purchased from Aladdin Reagent Database Inc. (Shanghai, China). All reagents are analytical grade and were used without further purification. All experiments were performed using ultra-pure water purified by the Milli-M system (Milford, MA).

2.2. Synthesis of BiOCl: QA-BiOCl-NF was prepared by solvothermal method. About 0.1 ml HCl and 0.5 mM $Bi(NO_3)_3{\cdot}5H_2O$ were dissolved in 10 and 40 ml ethylene glycol, respectively. They were mixed under continuous stirring for 60 min at room temperature and then transferred to an 80 ml teflon autoclave. After that, the autoclave was reacted for 24 h at 180°C and cooled down to room temperature. Finally, the product was cleaned by deionised water and absolute ethanol for several times. QA-BiOCl-NFs were obtained by freeze drying at −45°C for 12 h.

2.3. Photocatalytic activity measurement: The photocatalytic activity of the samples was evaluated by RhB degradation under visible light. For photocatalytic degradation under visible light, a 500 W xenon lamp (λ>400 nm) was used as the analogue light source with a light source spacing of ∼20 cm. About 50 mg catalyst was dispersed in 100 ml 10 mg/l RhB solution and treated by ultrasonic wave for 5 min to achieve adsorption–desorption equilibrium. Then, 0.1 ml H_2O_2 was added under continuous stirring and irradiation conditions. About 3 ml aliquots were collected every 1 min. Then, the degradation of RhB was determined by centrifugation at 13,500 rpm for 1 min. The absorption peak (AP) at 554 nm was measured by UV spectrophotometer.

2.4. Reduction of 4-NP: The reduction reaction of 4-NP in the range of 200–800 nm was studied by UV–visible (UV–vis) absorption spectroscopy. About 0.3 g $NaBH_4$ was dissolved in water to 20 ml, then mixed with 20 ml 12.5 mM 4-NP, stirred for 10 min, and finally added with 25 mg catalyst. Absorbance is measured every 10 s. The AP at 400 nm was measured by UV spectrophotometer.

2.5. Instruments and methods: The surface morphology of the sample was examined with an MIRA3 XMU/XMH scanning electron microscope (SEM) (TESCAN). Transmission electron microscope (TEM) image was obtained using a JEOL JEM-2010F. The crystal phase of the sample was identified using a Bruker D8 Advance X-ray diffractometer (XRD). UV–vis spectroscopy (UV) was examined with U-3900H Spectrophotometer (Hitachi). Electron spin resonance (ESR) test was measured by Bruker E500 ESP spectrometer. Total organic carbon (TOC) was obtained with multi N/C 3100.

3. Results and discussion: The SEM images of QA-BiOCl-NFs are shown in Fig. 1. As shown in Fig. 1, the BiOCl samples show the uniform size. To confirm the morphology of the nanosheets and get more details, TEM is shown in Fig. 2. Fig. 2*a* reveals the size of the nanosheets is about 220×220 nm. In Fig. 2*b*, the high-resolution TEM (HRTEM) image taken from

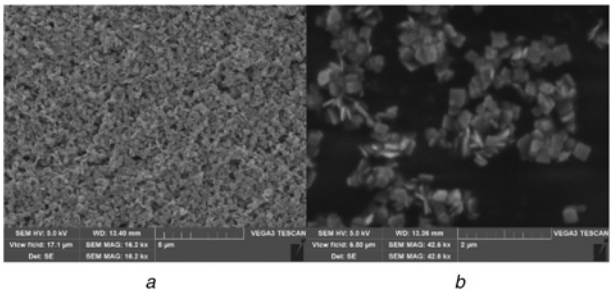

Fig. 1 *SEM images of QA-BiOCl-NFs (A, B)*

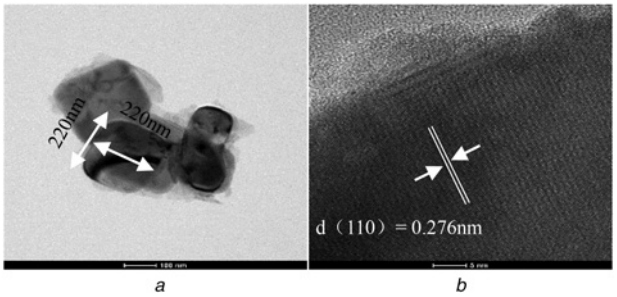

Fig. 2 *QA-BiOCl-NFs*
a TEM images
b HRTEM pattern

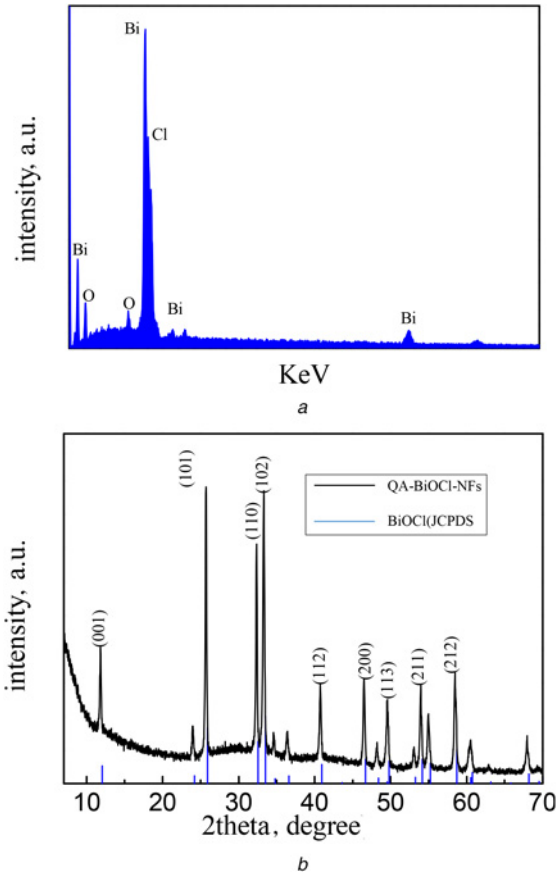

Fig. 3 *Patterns of QA-BiOCl-NFs*
a Energy dispersive X-ray spectroscopy
b XRD

QA-BiOCl-NFs displays a lattice fringe with the interplanar spacing of 0.276 nm, corresponding to the (110) plane of BiOCl.

As shown in Fig. 3*a*, the peaks from Bi, Cl and S confirm the presence of these elements in the QA-BiOCl-NFs sample. Fig. 3*b* shows the XRD measurement of the sample. All the sharp diffraction peaks can be well-indexed to the tetragonal structure of BiOCl (JCPDS Card No. 06-0249). The major diffraction peaks with 2θ values at 25.863°, 32.496° and 33.445° are indexed as (1 0 1), (1 1 0) and (1 0 2) crystal planes, respectively. No other peaks in the patterns are linked to the other impurities, demonstrating the high purity of the sample.

The reaction process and catalytic efficiency were monitored by UV–vis absorption spectroscopy. The continuous scanning wavelength is 200–800 nm. Initially, the aqueous solution of 4-NP was light yellow. When a certain concentration of freshly prepared $NaBH_4$ solution was added, the solution immediately changed from light yellow to bright yellow. The maximum AP of the solution without $NaBH_4$ is 319 nm, which belongs to the characteristic AP of 4-NP. When $NaBH_4$ was added, the maximum AP of the solution red-shifted from 319 to 400 nm due to the change of pH value, which is attributed to the characteristic AP of 4-NP in anionic state under alkaline condition. With the addition of a certain concentration of catalyst, the characteristic yellow of 4-NP faded quickly and the final solution became colourless.

As shown in Fig. 4*a*, the characteristic peak of 4-NP at 400 nm decreases rapidly until it disappears at 30 s and a new 4-AP AP is obtained at 300 nm. Without catalyst in Fig. 4*b* (a), the intensity of the AP does not change significantly even if $NaBH_4$ is excessive. It also shows that the reduction of 4-NP to 4-AP is not easy without catalyst. Moreover, line b indicates that the relationship between ln (C_t/C_0) and time is approximately linear in the presence of QA-BiOCl-NFs. Fig. 4*c* studies the degradation rate of 4-NP with different concentrations at 5 s, where A_t is the concentration of 4-NP at the time of measurement and A_0 is the initial concentration before measurement. Until the concentration reaches 4 mM, the degradation rate reaches 100%. It takes <5 s when the concentration is <4 mM, which is obviously higher than that of conventional catalysts.

In the presence of QA-BiOCl-NFs, the possible mechanism of $NaBH_4$ reducing 4-NP to 4-AP is as follows. First, BH_4^- is chemisorbed on the surface of the catalyst flake structure, then electrons are transferred from BH_4^- to QA-BiOCl-NFs, and finally 4-NP molecule can accept electrons and convert them into 4-AP [25].

In Table 1, the catalytic activity of QA-BiOCl-NFs is much higher than that of catalysts containing noble metals. It also shows that QA-BiOCl-NFs has excellent catalytic activity for borohydride-assisted reduction of 4-NP and is expected to be a good substitute for precious metal catalysts in the future.

The photocatalytic activity of the prepared QA-BiOCl-NFs was also investigated. Fig. 5*a* shows the change of photodegradation rate of RhB with time. RhB is nearly completely degraded in 20 min. This effect is better than the reported catalysts (Table 2). The percentage of degradation rate (A_t/A_0) relative to the degradation time is shown in Fig. 5*b*, where A_t is the concentration of RhB after irradiation and A_0 is the initial concentration before irradiation after the addition of QA-BiOCl-NFs to the solution. The degradation kinetics of Rh-B on QA-BiOCl-NFs follows a pseudo-first-order process. In the absence of irradiation, the A_t/A_0 almost does not decline, showing that the adsorption has little effect on the degradation rate. In addition, the photocatalytic activity of BiOCl decreased after three times of operation, where 1 h is needed for a nearly complete degradation. Obviously, this cost-less catalyst is suitable for the disposable use.

ESR spectroscopy is used to study the mechanism for detecting the production of ·OH and $\cdot O_2^-$. As shown in Fig. 6, after visible light irradiation, ·OH and $\cdot O_2^-$ signals appear, but under the same conditions, no signals are detected for the dark. Thus, the

doi: 10.1049/mnl.2018.5632

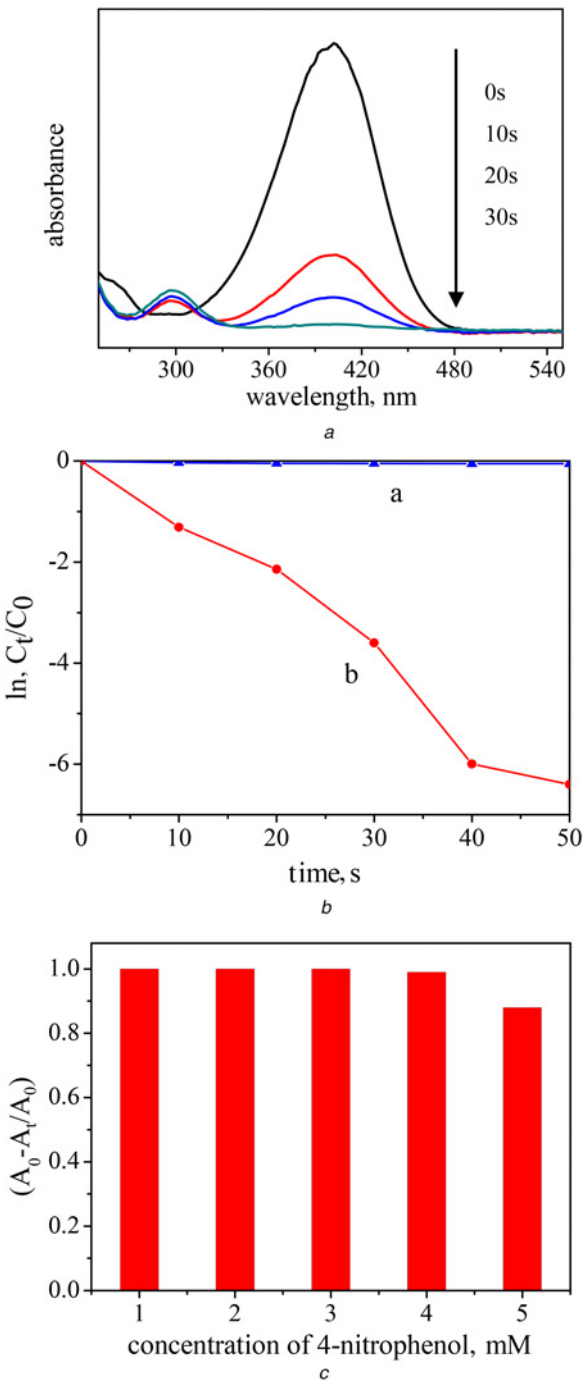

Fig. 4 *Characteristic peak of 4-NP*
a Time-dependent UV–vis absorption spectra for the reduction of 4-NP with QA-BiOCl-NFs
b Degradation efficiency of 4-NP as a function of time by QA-BiOCl-NFs (b) and blank (a)
c Degradation rate of 4-NP with different concentrations at 10 s

Table 1 Comparison of 4-NP on various noble metal catalysts

	4-NP, mM	$NaBH_4$, mM	Time, s	References
QA-BiOCl-NFs	5	0.16	30	herein
Pd–Ni	5	0.03	400	[26]
Ag–Au	4.67	0.67	360	[27]
Au–Ag	0.1	6.67	>1800	[28]

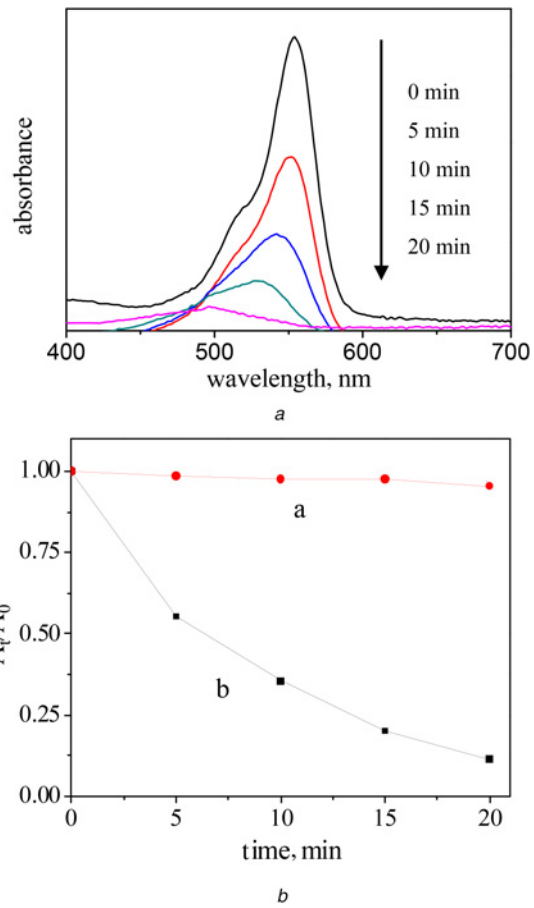

Fig. 5 *Change of photodegradation rate of RhB with time*
a UV–vis absorbance of RhB by the photocatalytic degradation of QA-BiOCl-NFs
b Degradation efficiency of RhB as a function of time by QA-BiOCl-NFs under visible light (b) and dark (a)

Table 2 Photocatalytic performance of some typical catalysts reported previously

	RhB, mg/l	Catalyst, mg/l	Time, s	References
QA-BiOCl-NFs	10	500	20	herein
Bi_2S_3/BiOCl	10	600	>80	[29]
Bi_2WO_6/Bi	20	500	>30	[30]
Bi_2WO_6	4.8	1000	>50	[31]

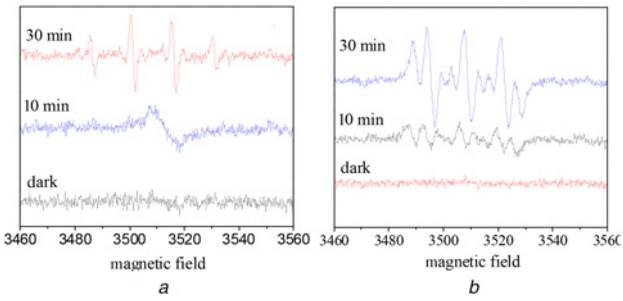

Fig. 6 *ESR spectra of*
a $\cdot O_2^-$ in QA-BiOCl-NFs aqueous solution irradiated by visible light
b ·OH in QA-BiOCl-NFs aqueous solution irradiated by visible light

photocatalytic process of QA-BiOCl-NFs is affected by ·OH and $\cdot O_2^-$. Under visible light irradiation with energy larger than QA-BiOCl-NFs bandgap, electrons in valence band are stimulated into conductive band, leaving holes in valence band. These photogenerated electrons and holes cause reductive and oxidative reactions, respectively [21, 32]. In other words, the degradation process of RhB can be described as follows:

$$\mathrm{BiOCl} + h\nu \rightarrow \mathrm{BiOCl}(\mathrm{e}^-) + \mathrm{BiOCl}(\mathrm{h}^+) \quad (1)$$

$$\mathrm{h}^+ + \mathrm{OH}^- \rightarrow \cdot\mathrm{OH} \quad (2)$$

$$\mathrm{H_2O_2} + \mathrm{e}^- + \mathrm{H}^+ \rightarrow \cdot\mathrm{OH} + \mathrm{H_2O} \quad (3)$$

$$\mathrm{H_2O_2} + \mathrm{h}^+ \rightarrow 2 \cdot \mathrm{OH} \quad (4)$$

$$\mathrm{O_2} + \mathrm{e}^- \rightarrow \cdot\mathrm{O_2^-} \quad (5)$$

$$\cdot\mathrm{OH}/\cdot\mathrm{O_2^-}/\mathrm{h}^+ + \text{dyes} \rightarrow \text{degradation products} \quad (6)$$

The comparison of QA-BiOCl-NFs with the reported catalysts in Table 2 shows that QA-BiOCl-NFs have excellent photocatalytic activity. Taking TOC as mineralisation index, the photodegradation performance of the dye was further studied. Within 20 min under visible light, the photodegradation rate of RhB was 64%, which indicated that the dye could achieve photodegradation effect. Therefore, QA-BiOCl-NFs material is a kind of catalyst with excellent photocatalytic activity.

4. Conclusions: In summary, a simple hydrothermal method was used for the preparation of BiOCl square nanosheets, which can be used as a new catalyst for the reduction of 4-NP and the degradation of organic dye RhB. It is demonstrated that QA-BiOCl-NFs have good catalytic activity for the degradation of 4-NP, and it can completely degrade 4-NP within 30 s. Its activity even exceeds platinum, gold and other noble metal catalysts.

5 References

[1] Chen M., Yu S., Zhang X., *ET AL.*: 'Insights into the photosensitivity of BiOCl nanoplates with exposing {001} facets: the role of oxygen vacancy', *Superlattices Microstruct.*, 2016, **89**, pp. 275–281

[2] Arthur R.B., Bonin J.L., Ardill L.P., *ET AL.*: 'Photocatalytic degradation of ibuprofen over BiOCl nanosheets with identification of intermediates', *J. Hazard. Mater.*, 2018, **358**, pp. 1–9

[3] Chen G., Zhu M., Wei X.: 'Photocatalytic properties of attached BiOCl-(0 0 1) nanosheets onto AgBr colloidal spheres toward Mo and Rh B degradation under an LED irradiation', *Mater. Lett.*, 2018, **212**, pp. 182–185

[4] Jiang J., Zhao K., Xiao X., *ET AL.*: 'Synthesis and facet-dependent photoreactivity of BiOCl single-crystalline nanosheets', *J. Am. Chem. Soc.*, 2012, **134**, (10), pp. 4473–4476

[5] Stephenson J., Celorrio V., Tiwari D., *ET AL.*: 'Photoelectrochemical properties of BiOCl microplatelets', *J. Electroanal. Chem.*, 2018, **819**, pp. 171–177

[6] Xie F., Mao X., Fan C., *ET AL.*: 'Facile preparation of Sn-doped BiOCl photocatalyst with enhanced photocatalytic activity for benzoic acid and rhodamine B degradation', *Mater. Sci. Semicond. Process.*, 2014, **27**, pp. 380–389

[7] Hao M., Fa D., Qian L., *ET AL.*: 'Ultrafine nanoparticles of Bi_2WO_6/$NiWO_4$ exhibiting high photocatalytic degradation toward Rh B', *J. Mater. Sci., Mater. Electron.*, 2017, **28**, (23), pp. 18145–18153

[8] Cai Y., Li D., Sun J., *ET AL.*: 'Synthesis of BiOCl nanosheets with oxygen vacancies for the improved photocatalytic properties', *Appl. Surf. Sci.*, 2018, **439**, pp. 697–704

[9] Li H., Zhang L.: 'Photocatalytic performance of different exposed crystal facets of BiOCl', *Curr. Opin. Green Sustain. Chem.*, 2017, **6**, pp. 48–56

[10] López Cuellar E., Olivares Cortéz J., Martínez-de la Cruz A., *ET AL.*: 'Photocatalytic activity of BiOCl thin films deposited by thermal evaporation', *Thin Solid Films*, 2018, **659**, pp. 57–63

[11] Wang P.-Q., Liu J.-Y., Hu Y.-Q., *ET AL.*: 'N, C-codoped BiOCL flower-like hierarchical structures', *Micro Nano Lett.*, 2012, **7**, (9), pp. 876–879

[12] Liu Q.Y., Han G., Zheng Y.F., *ET AL.*: 'Synthesis of $BiOBr_xI_{1-x}$ solid solutions with dominant exposed {0 0 1} and {1 1 0} facets and their visible-light-induced photocatalytic properties', *Separation Purification Technol.*, 2018, **203**, pp. 75–83

[13] Liu W., Qiao L., Zhu A., *ET AL.*: 'Constructing 2d BiOCL/C_3N_4 layered composite with large contact surface for visible-light-driven photocatalytic degradation', *Appl. Surf. Sci.*, 2017, **426**, pp. 897–905

[14] Zheng Y., Shu J., Wang Z.: 'AgCl@Ag composites with rough surfaces as bifunctional catalyst for the photooxidation and catalytic reduction of 4-nitrophenol', *Mater. Lett.*, 2015, **158**, pp. 339–342

[15] Bordbar M., Negahdar N., Nasrollahzadeh M.: '*Melissa officinalis* L. leaf extract assisted green synthesis of CuO/ZnO nanocomposite for the reduction of 4-nitrophenol and rhodamine B', *Separation Purification Technol.*, 2018, **191**, pp. 295–300

[16] Ikhsan N.I., Rameshkumar P., Huang N.M.: 'Controlled synthesis of reduced graphene oxide supported silver nanoparticles for selective and sensitive electrochemical detection of 4-nitrophenol', *Electrochim. Acta*, 2016, **192**, pp. 392–399

[17] Borah B.J., Bharali P.: 'Surfactant-free synthesis of CuNi nanocrystals and their application for catalytic reduction of 4-nitrophenol', *J. Mol. Catal. A, Chem.*, 2014, **390**, pp. 29–36

[18] Guo M., He J., Li Y., *ET AL.*: 'One-step synthesis of hollow porous gold nanoparticles with tunable particle size for the reduction of 4-nitrophenol', *J. Hazardous Mater.*, 2016, **310**, pp. 89–97

[19] Liu X., Li X., Qin L., *ET AL.*: 'CO_3O_4/CoP composite hollow polyhedron: a superior catalyst with dramatic efficiency and stability for the room temperature reduction of 4-nitrophenol', *Appl. Surf. Sci.*, 2018, **434**, pp. 967–974

[20] Hao M., Meng X., Miao Y.: 'Synthesis of $NiWO_4$ powder crystals of polyhedron for photocatalytic degradation of rhodamine', *Solid State Sci.*, 2017, **72**, pp. 103–108

[21] Hao M., Fa D., Qian L., *ET AL.*: 'WO_3@Bi_2WO_6/$NiWO_4$ nanocomposites with outstanding visible-light-driven photocatalysis for the degradation of organic dyes', *J. Nanosci. Nanotechnol.*, 2018, **18**, pp. 4788–4797(4710)

[22] Li K., Liang Y., Yang J., *ET AL.*: 'Controllable synthesis of {001} facet dependent four square BiOCl nanosheets: a high efficiency photocatalyst for degradation of methyl orange', *J. Alloys Compd.*, 2017, **695**, pp. 238–249

[23] Liang Z., Zhou C., Yang J., *ET AL.*: 'Visible light responsive Bi_2WO_6/BiOCL heterojunction with enhanced photocatalytic activity for degradation of tetracycline and rhodamine B', *Inorg. Chem. Commun.*, 2018, **93**, pp. 136–139

[24] Cao G.S., Wang G.L., Liu M.X., *ET AL.*: 'Photocatalytic removal of rhodamine B using Fe_3O_4/BioBr magnetic microsphere under visible-light irradiation', *Micro Nano Lett.*, 2015, **10**, (2), pp. 115–118

[25] Shi X., Zheng F., Yan N., *ET AL.*: '$CoMn_2O_4$ hierarchical microspheres with high catalytic activity towards P-nitrophenol reduction', *Dalton Trans.*, 2014, **43**, (37), pp. 13865–13873

[26] Revathy T.A., Dhanapal K., Dhanavel S., *ET AL.*: 'Pulsed electrodeposited dendritic Pd–Ni alloy as a magnetically recoverable nanocatalyst for the hydrogenation of 4-nitrophenol', *J. Alloys Compd.*, 2018, **735**, pp. 1703–1711

[27] Hareesh K., Joshi R.P., Sunitha D.V., *ET AL.*: 'Anchoring of Ag–Au alloy nanoparticles on reduced graphene oxide sheets for the reduction of 4-nitrophenol', *Appl. Surf. Sci.*, 2016, **389**, pp. 1050–1055

[28] Arora N., Mehta A., Mishra A., *ET AL.*: '4-nitrophenol reduction catalysed by Au–Ag bimetallic nanoparticles supported on Ldh: homogeneous vs. heterogeneous catalysis', *Appl. Clay Sci.*, 2018, **151**, pp. 1–9

[29] Cao J., Xu B., Lin H., *ET AL.*: 'Novel Bi_2S_3-sensitized BiOCl with highly visible light photocatalytic activity for the removal of rhodamine B', *Catal. Commun.*, 2012, **26**, (26), pp. 204–208

[30] Zhang X., Yu S., Liu Y., *ET AL.*: 'Photoreduction of non-noble metal Bi on the surface of Bi_2WO_6 for enhanced visible light photocatalysis', *Appl. Surf. Sci.*, 2016, **396**, pp. 652–658

[31] Han T., Wang X., Ma Y., *ET AL.*: 'Mesoporous Bi_2WO_6 sheets synthesized via a sol–gel freeze-drying method with excellent photocatalytic performance', *J. Sol-Gel Sci. Technol.*, 2016, **82**, (1), pp. 1–8

[32] Chang J.-Q., Zhong Y., Hu C.-H., *ET AL.*: 'Synthesis and significantly enhanced visible light photocatalytic activity of BiOCl/AgBr heterostructured composites', *Inorg. Chem. Commun.*, 2018, **96**, pp. 145–152

doi: 10.1049/mnl.2018.5632